Modeling of associative ionization reactions in hypersonic rarefied flows

By I. D. Boyd †

1. Motivation and objectives

The aerothermodynamics analysis of the high altitude portions of a hypersonic entry trajectory are routinely performed using the direct simulation Monte Carlo (DSMC) method (Bird 1994). For example, the DSMC technique has been applied in the past to analyze hypersonic air flows at velocities up to about 10 km/s Bird (1987); Boyd & Gokcen (1994). These studies included ionizing reactions using procedures for simulating the electrons in DSMC proposed by Bird (1987). An attempt by Bird (1989) to assess these electron simulation schemes by comparing with experimental measurements made in a hypersonic flight was unsuccessful in part due to the limited computer resources available at the time.

The primary goal of this study is to develop and apply new numerical schemes to improve the ability of the DSMC method to simulate the plasma layer formed around a hypersonic vehicle entering the atmosphere at orbital velocity under rarefied flow conditions. The simulations are required for assessment of communications blackout mitigation schemes. Using modern computers, it is now possible to assess these schemes using the same available flight measurements considered in Bird (1989).

The Radio Attenuation Measurement (RAM) experiments involved a series of hypersonic entry flights designed to study communications blackout. The vehicle of interest here (RAM-C II) consisted of a cone with a spherical nose cap of radius, R_N=0.1524 m, a cone angle of 9 °, and a total length of approximately 1.3 m. While entering at orbital velocity (7.8 km/s), the RAM-C II experiment made measurements from approximately 90 km to 60 km altitude. Electron number density was measured using two different diagnostics at several locations in the plasma layer surrounding the vehicle Grantham (1970); Linwood-Jones & Cross (1972). A series of reflectometers was used to measure the maximum plasma density along lines normal to the vehicle surface in four different locations. A rake of Langmuir probes measured variation in the plasma density across the plasma layer at a location Z/R_N=8.1, near the rear of the vehicle. A schematic diagram of the vehicle geometry and the instrumentation placement is shown in Fig. 1.

The RAM-C II data have been used in several previous CFD studies, e.g. Candler & MacCormack (1991); Josyula & Bailey (2003); Scalabrin & Boyd (2006) to assess ionization models. Bird (1989) attempted to use the DSMC method to study the RAM-C II data collected at 81 km but obtained inconclusive results in part due to the inability to use a large enough number of particles given the computer resources of that time. Note that Bird's study was conducted more than 15 years ago. The CFD analyses of the 81 km RAM-C II flow indicate that the mole fraction of electrons ranges from about 10^{-3} and below. Resolving such a trace amount of any species with the DSMC technique requires special treatment. The present study again considers the 81 km RAM-C II data and seeks

† Current Address: Department of Aerospace Engineering, University of Michigan, Ann Arbor, MI 48109

to apply modern DSMC methods as well as faster computers to this flow configuration. The overall goal of the work is to produce a validated DSMC approach for addressing communications blackout issues at high altitude.

2. Simulation of ionizing reactions

The presence of electrons in a DSMC computation presents a couple of difficulties because their mass is five orders of magnitude lower than the heavy air species such as nitrogen and oxygen. First, if all species are equilibrated to the same translational temperature, due to their very low mass, the electrons diffuse at velocities that are more than two orders of magnitude higher than the air species. However, the strong electrostatic attraction between electrons and ions leads to significant limitation of the transport of the electrons. Indeed, the assumption of ambi–polar diffusion requires that electrons and ions diffuse at the same average rate. First proposed by Bird (1989), ambi-polar diffusion is implemented in the DSMC technique by forcing the motion of an electron to follow that of the ion with which it was first created in the simulation. This ambi–polar diffusion model is employed in the current work. Note that the DSMC implementation of ambi-polar diffusion affects the average motion of the electrons without affecting their thermal velocities.

The second problem created by the very small mass of an electron concerns simulation of collisions. The collision probability in the DSMC technique is proportional to the product of the collision cross-section and the relative velocity of a pair of particles. If one of the particles is an electron, then the pair will possess a very large relative velocity. Electrons therefore undergo a much higher rate of collisions in comparison to the heavy species. Thus, DSMC computations involving electrons either have to employ a time step that is significantly smaller than that needed for a simulation under the same flow conditions without electrons, or subcycling of collisions must be performed. In subcycling, the computation of collisions is broken down into several cycles for each overall simulation time step. Both of these approaches lead to a significant increase in overall computational cost in comparison to a simulation that does not involve electrons. In the results below, the possibility of alleviating this difficulty by artificially increasing the mass of the electron is investigated.

The third area of concern for the RAM-C II simulations concerns the level of ionization that is anticipated to be low. At orbital speed of 7.8 km/s, corresponding to an energy of about 9 eV, the main reactions leading to the production of charged species in air are the associative ionization reactions:

$$N + N \rightarrow {N_2}^+ + E^- \tag{2.1}$$

$$O + O \rightarrow {O_2}^+ + E^- \tag{2.2}$$

$$N + O \rightarrow NO^+ + E^-. \tag{2.3}$$

It should be noted that Bird (1989) only included the third of the three associative ionization reactions and his results generally under-predicted the electron number densities measured on RAM-C II by factors between two and ten.

In the DSMC technique, the Total Collision Energy (TCE) chemistry model (Bird 1994) converts chemical rate coefficients expressed in modified Arrhenius form into reaction probabilities. Using the rate coefficients recommended at high temperature by Park (1990), the reaction probabilities of these three reactions are plotted in Fig. 2. From this

plot, it can be seen that the activation energies for all three reactions lie below 9 eV, and that the reaction probabilities are relatively low.

In preliminary DSMC calculations of the RAM-C II flow, a very small number of these ionization reactions occurred, similar to the situation encountered in Bird's original study Bird (1989). It is therefore necessary to employ special numerical schemes in order to generate a sufficient number of charged particles (ions and electrons) in the RAM-C II flowfields. These schemes consist of the following steps:
(1) the reaction probabilities of the three associative ionization reactions are increased by a factor, R;
(2) whenever an ionizing reaction occurs, several realizations, $S > 1$, of the post-reaction outcome are processed;
(3) whenever an ionizing reaction occurs, the charged particles created are given a *relative* numerical weight of $1/(R \times S)$. The numerical weight of a particle in the DSMC technique is the number of real molecules represented by a single particle. Most DSMC computations employ the same numerical weight for all particles. However, for simulating species occurring in trace quantities, it is useful to decrease the relative numerical weight of trace species particles so that a larger number of such particles is simulated. The relative numerical weight is taken into account in computing the species number density and in determining the number of collisions experienced by these trace particles using the DSMC trace-species algorithm of Boyd (1996). This algorithm revises the No Time Counter method of Bird (1994) so that the number of pairs of particles to be formed between species i and species j is given by:

$$C_{i,j} = \frac{1}{2}\frac{N_i W_i}{V} N_j [\sigma g]_{max} \Delta t, \tag{2.4}$$

where N_i and N_j are the numbers of particles of species i and j, W_i is the numerical weight of species i, V is the cell volume, σ is the collision cross-section, g is the relative velocity, and Δt is the time step. For each of the $C_{i,j}$ particle pairs, the probability of collision is evaluated as:

$$P = \frac{\sigma g}{[\sigma g]_{max}} \tag{2.5}$$

where a separate maximum value is retained in each cell of the computational domain for each species pair $i - j$. When two particles of different numerical weights collide, the particle with the larger numerical weight is split into two. One of these particles is given the same numerical weight as the trace particle and the second split particle is given the numerical weight needed to preserve total mass. The two particles of equal numerical weight are then collided together using the standard DSMC collision steps. Following collision, each of the split particles is retained with the probabilities given by the ratio of their new and original numerical weights. This scheme conserves momentum and energy when averaged over many collisions and results are provided to illustrate the performance of the algorithm for this particular application. Full details of the procedures are provided in Boyd (1996) and further examples of their successful use can be found in Kossi & Boyd (1998); VanGilder & Boyd (2000).

In the simulations presented below, the ionizing reaction probabilities are increased by a factor of $R = 30$ (to make sure that the maximum probability is still less than one) and four post-collision outcomes are processed for each single ionization event ($S = 4$). Use of these special steps therefore makes it possible to increase the number of charged particles

in the DSMC computation by a factor of about 120. This is a sufficient increase to make it possible to obtain sufficient numerical resolution of the properties of the charged species.

The associative ionization reactions are also simulated in the reverse direction. As explained in Boyd & Gokcen (1994), the backward rates are expressed in modified Arrhenius form using the ratio of the forward rate coefficient and the equilibrium constant for each reaction. The forward and backward rate coefficients employed in the simulations are those used in Boyd & Gokcen (1994).

3. Details of the DSMC flow model

The current computations employ a DSMC code developed specifically for hypersonic, ionized flow simulations reported by Boyd & Gokcen (1994). The flow is simulated as an 11-species (N_2, N, O_2, O, NO, N_2^+, N^+, O_2^+, O^+, NO^+, E^-) reacting gas. Models are implemented for rotational Boyd (1990) and vibrational Boyd (1991) energy exchange. Most of the chemical reactions employ the TCE model except for the dissociation of nitrogen and oxygen. In some simulations, these reactions employ the Vibrationally Favored Dissociation (VFD) model of Haas & Boyd (1993). The VFD model makes it possible to bias the dissociation reaction probability in favor of molecules that possess a higher vibrational energy. In this way, the important phenomenon of vibration dissociation coupling can be simulated. In the present work, the VFD favoring parameter ϕ is set to 2.0 for nitrogen dissociation and 0.5 for oxygen dissociation, as determined in the prior work of Haas & Boyd (1993). As an illustration, Fig. 3 shows the VFD dissociation probabilities as a function of total collision energy and vibrational energy for nitrogen dissociation. Simulation of the dissociation reactions is a key element in simulating communications blackout because atoms are required to generate the charged particles via the associative ionization reactions. The sensitivity of the DSMC results to the dissociation modeling will be examined for the RAM-C II flow conditions.

The full list of chemical reactions and rate coefficients employed in the present study are those used in Boyd & Gokcen (1994). Note the omission in this study of the direct ionization reactions:

$$N + E^- \rightarrow N^+ + 2E^- \tag{3.1}$$

$$O + E^- \rightarrow O^+ + 2E^- \tag{3.2}$$

The activation energies for these reactions lie above 13 eV which is higher than the collision energies experienced in the RAM-C II flow. The absence in the RAM-C II flows of chemical reactions driven by electrons suggests that it may be possible to simplify the simulation of the electrons by artificially increasing their mass. This idea is investigated in the following section.

4. Results

DSMC computation of the flow around the RAM-C II vehicle is performed at a flow velocity of 7.8 km/s and flow conditions corresponding to 81 km altitude in the atmosphere. This is a point on the RAM-C II trajectory where measurements of electron number density are reported in Grantham (1970); Linwood-Jones & Cross (1972). At 81 km, the mean free path is about 0.005 m giving an overall Knudsen number for the flow of about 0.03 based on the spherical cap radius of RAM-C II. The analyses conducted in this study assume axial symmetry as the vehicle had a very small angle of

attack. The vehicle surface is assumed to be isothermal and diffuse at a temperature of 1500 K, is non-catalytic to atoms, but fully catalytic to charged species such that ions and electrons recombine to the neutral atom or molecule.

4.1. *Simulations of the nose cap region*

As discussed above, the presence of electrons in the flowfield creates problems for the DSMC technique. The particular problem related to the need to either decrease the time step or perform collision subcycling greatly increases the numerical cost of the DSMC computations. It is therefore of interest to see if the cost of DSMC computations of these hypersonic flow conditions can be reduced by artificially increasing the mass of the electrons. This approach is certainly not valid when electrons drive any of the chemistry. However, as indicated in the discussions above, earth entry at orbital speed is not sufficiently energetic to produce any direct ionization by electrons.

An initial test simulation is therefore employed on a subset of the entire RAM-C II flowfield representing the first 70 ° of the spherical cap of the cone, approximately midway between the locations of the first two reflectometers (R1 and R2) indicated in Fig. 1. This region includes the stagnation streamline where the temperatures are highest and where much of the air chemistry occurs. A mesh is generated of 179 by 109 cells where the latter direction goes around the body. The mesh is adapted such that all cells are smaller than the local mean free path. Two simulations are performed:
(1) the real electron mass is employed and the collision routine is subcycled 30 times each iteration; and
(2) the electron mass is increased by a factor of 1000 and no subcycling is employed.

The TCE model is employed for all chemical reactions including dissociation. The simulations employ about 350,000 particles at steady state and are performed for 50,000 iterations.

A general impression of the flowfield can be seen in Fig. 4, where contours of translational temperature are shown. The contours are plotted at intervals of 2000 K. These results are obtained from the simulation employing the real electron mass. A more quantitative understanding of the flowfield is provided in Figs. 5 and 6 in which profiles along the stagnation streamline of various properties are shown. In Fig. 5, the mole fractions of the major species are shown. In these plots, the free stream is on the left and the vehicle surface is on the right. The profiles illustrate the strong degree of chemical non-equilibrium present in these flows, with initial dissociation of molecular nitrogen and oxygen through the shock followed by partial recombination close to the vehicle surface. Figure 6 shows profiles of temperature of the translational, rotational and vibrational modes indicating a strong degree of thermal non-equilibrium.

The effect of artificially increasing the electron mass by a factor of 1000 is assessed in Figs. 7 and 8. In Fig. 7, the translational temperatures for the overall gas and for the electrons are shown. Consider first the overall and electron translational temperatures obtained with the real electron mass. The electrons exhibit a very strong degree of thermal non-equilibrium except in the region immediately adjacent to the surface. Electrons are created in the region where the translational temperature is highest. However, when electrons are created, they have little initial energy and become energized only through subsequent collisions.

The profiles obtained from the two different simulations show almost perfect agreement for the overall gas translational temperature. For the temperature of the electrons, the simulation employing the increased electron mass shows that some of the electrons are transported through the shock wave without undergoing a sufficient number of collisions.

Qualitatively, this phenomenon is expected since the increased electron mass must lead to a reduced collision rate of the electrons. The key question is whether this behavior leads to any significant differences in the electron number density, the key parameter for understanding communications blackout phenomena. This question is answered by Fig. 8, which shows the profiles along the stagnation streamline of the number densities of several species. Again, the profiles obtained from the two different simulations are compared and it is clear that very good agreement is obtained for all species shown. Significantly, the profiles of electron number density from the two simulations are in excellent agreement. In the front of the shock, the fact that the electron densities are so similar while the electron temperatures are so different is explained by the use of the ambi-polar diffusion assumption. Since the electrons are constrained to diffuse with the ions, the relatively poor simulation of their temperature with the increased electron mass does not significantly affect the overall transport of the electrons in the flowfield.

The variation in the number densities of molecular nitrogen, the electrons and the major ion species along the stagnation streamline is shown in Fig. 9. The profiles indicate that the mole fraction of electrons is indeed very small, being less than 0.1%. The ion profiles show that while NO^+ has the highest ion concentration, all three molecular ions contribute to the total plasma density and should be included in the simulation.

The profiles of maximum electron number density along line R1 normal to the vehicle surface are shown in Fig. 10 along with the single RAM-C II reflectometer data point. Clearly, good agreement is obtained between the two simulations and with the flight measurement.

The simulation performed with the increased electron mass requires a factor of about 10 less time to run on a computer when compared to the actual electron mass. In the latter case, the collision routine is called 30 times for every iteration. The collision routine accounts for about 30% of the cost of a single iteration without subcycling, thus reducing the overall overhead of subcycling. In conclusion, the results of the small-scale, nose cap simulations clearly indicate that accurate prediction of electron number density is possible under these flow conditions through artificially increasing the electron mass by a factor of 1000. The increased electron mass does lead to inaccuracies in simulation of the electron temperature, but that is relatively unimportant in assessment of communications blackout issues. The factor of 10 increase in computational efficiency provided by this approach is of great benefit in performing the DSMC computations for the full RAM-C II vehicle.

4.2. *Full vehicle simulations*

The computational domain for the full-scale simulation is shown in Fig. 1 and employs a mesh that consists of 179 (toward the body) by 864 (along the body) cells. Once again, the mesh is adapted to ensure that each cell is smaller than the local mean free path. Each simulation employs the electron mass artificially increased by a factor of 1000. The simulations employ more than three million particles and are run for 150,000 iterations. Results are presented below for both the TCE and VFD chemistry models for the dissociation reactions. All other reactions employ the TCE model.

The overall flowfield contours of translational temperature are shown in Fig. 11. The contours reveal both the strong compression in front of the vehicle and the subsequent expansion of the flow around the shoulder of the spherical nose cap. Contours of the electron number density are shown in Fig. 12. There is a more than two orders of magnitude reduction in electron number density as a streamline is followed from the stagnation region around the side of the vehicle. This behavior is expected due to a combination of

the gas expansion process but also due to the weaker compression across the outer edges of the bow shock wave. Some statistical scatter is evident in the low density contours due to relatively small numbers of electron particles that are created even when using the special numerical techniques discussed earlier.

The variation of the maximum electron number density evaluated along the four lines (R1–R4) normal to the vehicle surface is shown in Fig. 13. Simulation profiles obtained with both the TCE and VFD chemistry models are compared with the RAM-C II flight data. Some sensitivity of the predicted profiles of electron number density to the dissociation model is apparent. The electron number density predicted with the VFD model is consistently about a factor of two lower than that obtained with the TCE model. The VFD model simulates a decreased dissociation rate when the vibrational temperature is below the translational temperature, which is the case in compressed hypersonic flows. This phenomenon is illustrated in Fig. 14, which shows the profiles of nitrogen and oxygen atoms along the stagnation streamline computed using the TCE and VFD models for the dissociation reactions. The concentrations of both nitrogen and oxygen atoms predicted by the VFD model are again about a factor of two lower than that obtained with the TCE model. This reduction in atomic concentrations leads directly to a reduction in the production of electrons through the associative ionization reactions. No error bars for the RAM-C II reflectometer data are provided in Grantham (1970) but it is reasonable to conclude that both DSMC profiles provide very good agreement with the measurements.

Figure 15 shows comparisons between the RAM-C II flight measurements and the two different DSMC computations for the profile of electron number density across the plasma layer at the downstream end of the vehicle (line L1 is Fig. 1). The RAM-C II data in this case were obtained with a rake of Langmuir probes Linwood-Jones & Cross (1972). As reported in Linwood-Jones & Cross (1972), the RAM-C II vehicle experienced a coning motion during re-entry with a rate of about three revolutions per second, which gave rise to variation in the electron number density measured by the Langmuir probes. The error bars included in Fig. 15 for the measured data represent the variations experienced for these probes at 81 km for one complete revolution. The DSMC results again demonstrate sensitivity of the predicted electron number density to the two different dissociation models with the VFD model predicting an electron number density that is about a factor of two lower than the TCE model. Given the difficulties and uncertainties in making measurements in hypersonic flight conditions, the level of agreement for either DSMC result with the RAM-C II data can be considered very good.

The degree of ionization as a function of distance from the wall (S) along each of the four lines (R1–R4 in Fig. 1) is shown in Fig. 16. As the plasma flows around the vehicle, the peak level of ionization monotonically diminishes. This trend is explained by two physical mechanisms. First, the highest levels of ionization occur on the stagnation streamline where the highest temperatures are generated that provide the peak rates of dissociation and ionization. The temperatures are highest in this region because the bow shock is essentially a normal shock on the stagnation streamline leading to maximum compression. Away from the stagnation streamline, the streamlines pass through significantly weaker oblique shocks that form the bow shock around the vehicle. These weaker shocks generate significantly lower temperatures and associated rates of dissociation and ionization. In addition, there is gas dynamic cooling of the flow as it expands around the shoulder of the vehicle. The temperature profiles shown in Fig. 11 confirm these phenomena. The second mechanism leading to a reduction in degree of ionization from location R1 to R4 is the assumption in the computations that all charged species

recombine on the surface. Thus, a significant fraction of the ions and electrons created in the stagnation streamline region are consumed by the vehicle wall.

5. Acknowledgements

This work was performed during a sabbatical leave at the Center for Turbulence Research at Stanford University, from which financial support is gratefully acknowledged.

REFERENCES

Bird, G. A.1987 Nonequilibrium Radiation During Re-entry at 10 km/s. *AIAA Paper 87-1543*.

Bird, G. A.1989 Computation of Electron Density in High Altitude Re-entry Flows. *AIAA Paper 89-1882*.

Bird, G. A.1994 *Molecular Gas Dynamics and the Direct Simulation of Gas Flows* Oxford University Press, Oxford.

Boyd, I. D.1990 Analysis of Rotational Nonequilibrium in Standing Shock Waves of Nitrogen. *AIAA J.* **28**, 1997-1999.

Boyd, I. D.1991 Analysis of Vibrational-Translational Energy Transfer Using the Direct Simulation Monte Carlo Method. *Phys. Fluids A* **3**, 1785-1793.

Boyd, I. D.1996 Conservative Species Weighting Scheme for the Direct Simulation Monte Carlo Method. *J. Thermophys. Heat Transfer* **10** 579-587.

Boyd, I. D. & Gokcen, T.1994 Computation of Axisymmetric and Ionized Hypersonic Flows Using Particle and Continuum Method. *AIAA J.* **32**, 1828-1835.

Candler, G. V. & MacCormack, R. W.1991 Computation of Weakly Ionized Hypersonic Flows in Thermochemical Nonequilibrium. *J. Thermophys. Heat Transfer* **5**, 266-272.

Grantham, W. L.1970 Flight Results of a 25000 Foot Per Second Reentry Experiment Using Microwave Reflectometers to Measure Plasma Electron Density and Standoff Distance. *NASA Technical Note D-6062*.

Haas, B. L. & Boyd, I. D.1993 Models for Direct Monte Carlo Simulation of Coupled Vibration-Dissociation. *Phys. Fluids A* **5**, 478-488.

Josyula, E. & Bailey, W.2003 Governing Equations for Weakly Ionized Plasma Flowfields of Aerospace Vehicles. *J. Spacecr. Rockets* **40**, 845-853.

Kossi, K. K., Boyd, I. D. & Levin, D. A.1998 Direct Simulation of High Altitude Ultra-Violet Emission From the Hydroxyl Radical. *J. Thermophys. Heat Transfer* **12**, 223-232.

Linwood-Jones, W. & Cross, A. E.1972 Electrostatic Probe Measurements of Plasma Parameters for Two Reentry Flight Experiments at 25000 Feet Per Second. *NASA Technical Note D-6617*.

Park, C.1990 *Nonequilibrium Hypersonic Aerothermodynamics* Wiley, New York.

Scalabrin, L. C. & Boyd, I. D.2006 Numerical Simulation of Weakly Ionized Hypersonic Flow for Reentry Configurations. AIAA Paper 2006-3773.

VanGilder, D. G., Boyd, I. D., & Keidar, M.2000 Particle Simulations of a Hall Thruster Plume. *J. Spacecr. Rockets* **37**, 129-136.

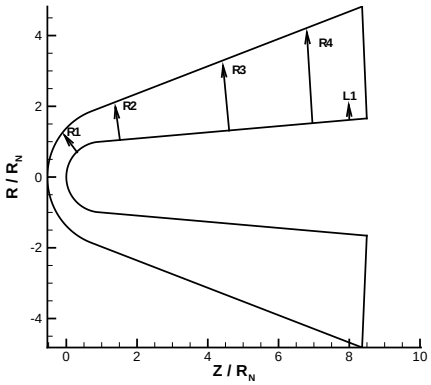

FIGURE 1. Computational domain for flow around the RAM-C II vehicle including the locations of the reflectometers (R1–R4) and the rake of Langmuir probes (L1).

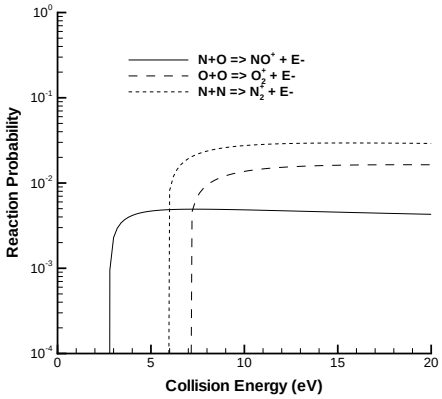

FIGURE 2. Probability of associative ionization as a function of collision energy obtained with the TCE model.

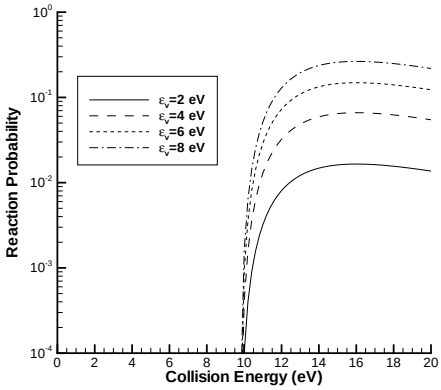

FIGURE 3. Probability of dissociation obtained with the VFD model for nitrogen dissociation.

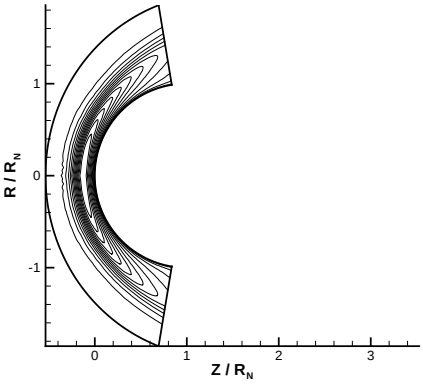

FIGURE 4. Contours of translational temperature (K) for the RAM-C II nose cap region simulation.

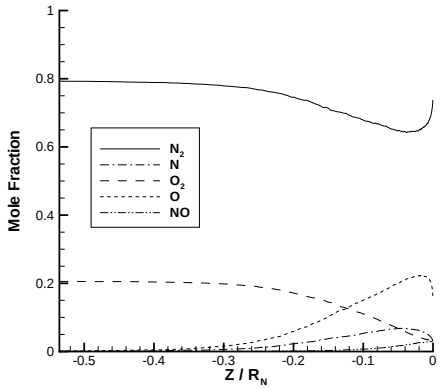

FIGURE 5. Mole fraction profiles along the stagnation streamline for the RAM-C II nose cap region simulation.

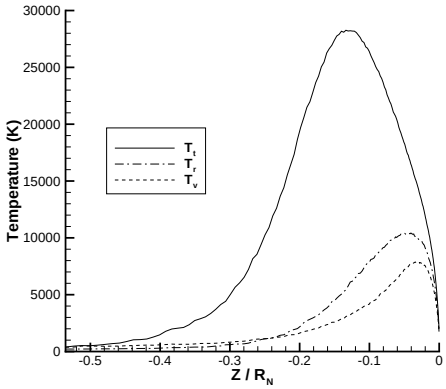

FIGURE 6. Temperature profiles along the stagnation streamline for the RAM-C II nose cap region simulation.

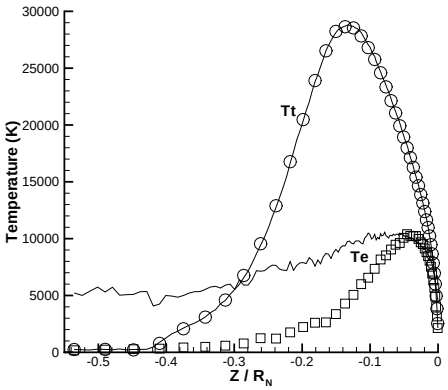

FIGURE 7. Temperature profiles along the stagnation streamline for the RAM-C II nose cap region simulation: lines=reduced electron mass.

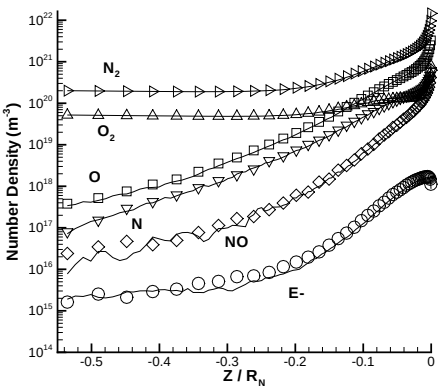

FIGURE 8. Species number density profiles along the stagnation streamline for the RAM-C II nose cap region simulation: lines=reduced electron mass.

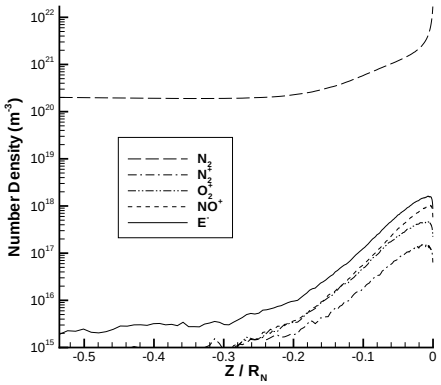

FIGURE 9. Number density profiles of various species along the stagnation streamline for the RAM-C II nose cap region simulation.

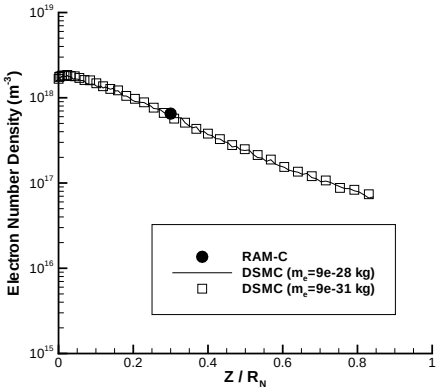

FIGURE 10. Maximum electron number density as a function of distance along the RAM-C II vehicle.

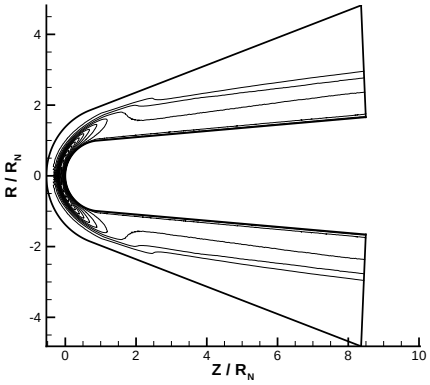

FIGURE 11. Contours of translational temperature (K) for the full-scale RAM-C II simulation.

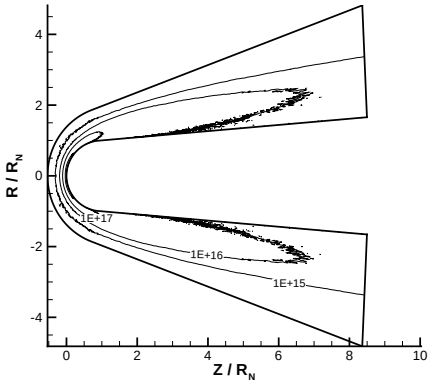

FIGURE 12. Electron number density contours (m^{-3}) for the full-scale RAM-C II simulation.

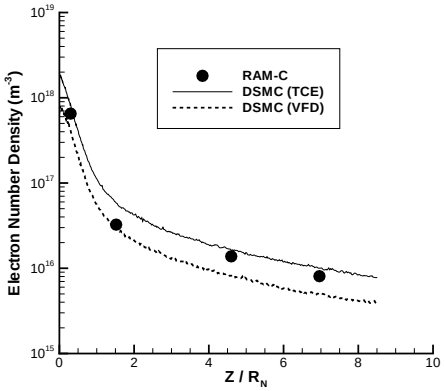

FIGURE 13. Maximum electron number density as a function of distance along the RAM-C II vehicle.

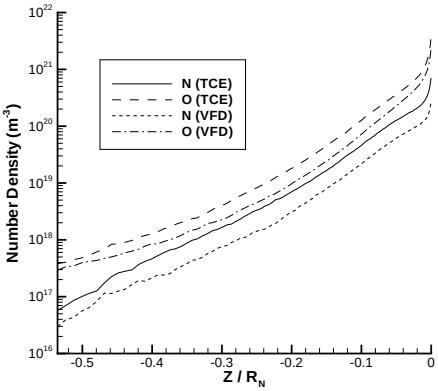

FIGURE 14. Profiles of atom number density obtained along the stagnation streamline with two different chemistry models.

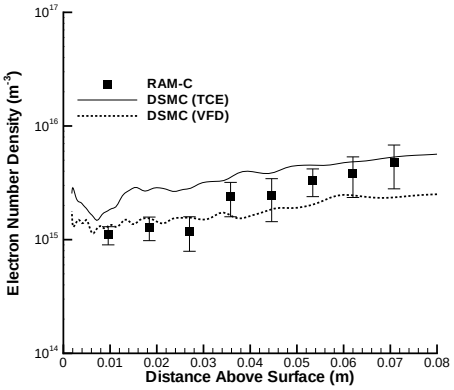

FIGURE 15. Electron number density as a function of distance from the RAM-C II vehicle at the Langmuir probe location.

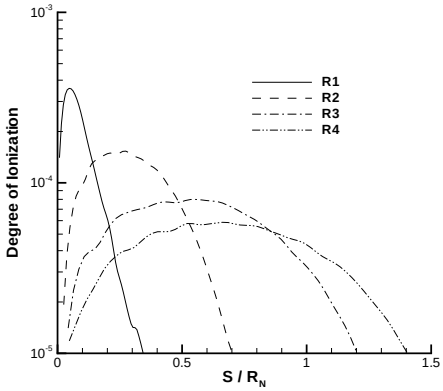

FIGURE 16. Profiles of ionization degree as a function of distance from the surface along the four reflectometer lines.